RSC Advances

PAPER

View Article Online
View Journal | View Issue

Cite this: *RSC Adv.*, 2017, **7**, 35111

Green synthesis of multi-metallic nanocubes†

Nabanita Patra,[a] Ashoka Chary Taviti,[bc] Anupam Sahoo,[d] Abhisek Pal,[a] Tushar Kant Beuria,*[c] Anindita Behera*[a] and Srikanta Patra *[d]

Received 15th May 2017
Accepted 3rd July 2017

DOI: 10.1039/c7ra05493a

rsc.li/rsc-advances

A facile synthetic route and growth mechanism of heterobimetallic cubical nanoparticles Au@AgCl and Ag@AgCl@Au have been developed using *Muntingia calabura* flower extract. The formation of nanoparticles has been confirmed through UV-Vis, powder X-ray diffraction and electron microscopy. The elemental composition of the nanoparticles has been evidenced by EDS analysis. Combing the UV-Vis spectral analysis and powder X-ray diffraction studies, the composition of bimetallic nanoparticles are assigned as Au@AgClNP and Ag@AgCl@AuNP. The prepared nanoparticles display good antibacterial activity which is comparable to standard kanamycin and ampicillin.

Introduction

An anisotropic structure of metallic nanoparticles attracts considerable research attention due to their interesting properties and widespread applications in the fields of catalysis, electronics, imaging, therapeutics, *etc.*[1–8] An anisotropic nanostructure can be achieved by controlling different parameters such as the reducing agent, stabilising agent, concentration ratio of reactants, reaction temperature, pH, *etc.*[9,10] Synthesis of anisotropic nanostructures with a high degree of control over the shape, size and composition using established conventional methods is a very difficult task as this involves multistep synthesis processes. In addition, in most of the cases the nanoclusters are prepared and stabilised by the utilisation of synthetic chemicals as reducing and stabilising agents which are hazardous or toxic and makes the nanoparticles bio-incompatible. Replacement of toxic chemicals by biomolecules or through biogenic processes would be an alternative and efficient strategy for the synthesis of nanoparticles to overcome the aforementioned limitations.[11–13] Among different living organism, plants are the best choice for their simplicity and easy handling.[11,14,15] Phytochemicals (polyphenols, terpenoids, flavones, *etc.*) with diverse range of reducing properties (mild or strong) present in different plant are responsible for the synthesis of metal nanoparticles.[16–20] The reducing-cum-capping/stabilisation properties of plant phytochemicals make the metal nanoparticles eco-friendly, cost effective and biocompatible. Considering these aspects, various research groups have used different plant extracts for the synthesis of shape and size-tunable metal nanoparticles using different metals salts (gold, silver, copper *etc.*) as precursor.[21–23] However, little progress has been made on the green synthesis of heterometallic core–shell nanoparticles. Although the heterometallic core–shell type nanoparticles often display improved or new properties as compared to their monometallic counterparts.[24,25] Moreover, bio-conjugated metal nanoparticles are known to exhibit improved pharmacological activities (antibacterial and anticancer activity and induction of angiogenesis) as compared to the individual counterpart.[23,24,26,27] Thus, green synthesised multimetallic nanoparticles using medicinal plant extract of definite physiological activity are anticipated to exhibit increased/new medicinal properties. However, a very little work has been done in this aspect. Moreover, to the best of our knowledge no reports have been found on the antibacterial activity of green synthesised shape selective heterometallic nanoparticles.

On the other hand, *Muntingia calabura* (MC) (family Elaeocarpaceae), also known as Jamaican Cherry (mainly seen in parking lot) are known for its medicinal values. In Southeast Asia, this plant is used as a folk medicine (*e.g.* fever, headaches, antidyspeptic, liver disease, antiseptic).[28–30] Aqueous extract of this plant, contains chalcones, alkaloids, proteins, flavonoids, saponin, tannin and anthraquinone have anti-nociceptive, anti-inflammatory and antipyretic activity.[31,32] Flavonoids present in MC exhibited significant antioxidant, anticancer and antibacterial activity.[33–35] In addition, the aforementioned plant metabolites containing the different functional groups such as phenolic–OH, $-NH_2$, –CHO, –COOH *etc.* are known for the bio-reduction and stabilisation of metal nanoparticles.[11,36–38] However, preparation of metal nanoparticles using the medicinally important MC flower extract has not been yet explored. Thus, considering this aspect the present contribution intends

[a]*School of Pharmaceutical Sciences, Siksha 'O' Anusandhan University, Sumpur, Bhubaneswar-751003, Orissa, India. E-mail: anindita02@gmail.com*

[b]*Manipal University, Manipal, Karnataka, 576104, India*

[c]*Institute of Life Sciences, Bhubaneswar, Odisha-751021, India. E-mail: tkbeuria@ils.res.in*

[d]*School of Basic Sciences, Indian Institute of Technology Bhubaneswar, Jatni, Odisha-752050, India. E-mail: srikanta@iitbbs.ac.in*

† Electronic supplementary information (ESI) available: Detailed experimental procedures and related data. See DOI: 10.1039/c7ra05493a

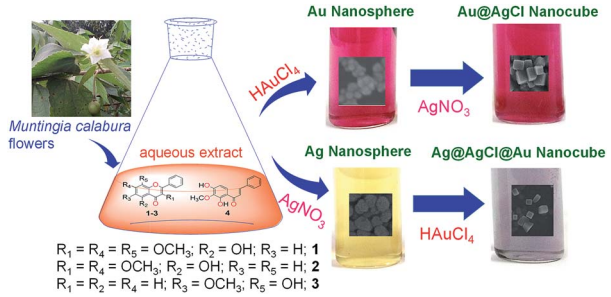

Scheme 1 Synthesis of metal nanoparticles using flower extract of *Muntingia calabura*.

to highlight the synthesis of mono and bimetallic nanoparticles using MC flower extract (Scheme 1).

Herein, we report a green chemistry approach for the synthesis of monometallic gold nanoparticles (AuNP, **NP1**) and silver nanoparticles (AgNP, **NP2**), and heterometallic cubical core–shell nanostructures Au@AgClNP (**NP3**) and Ag@AgCl@AuNP (**NP4**) by adding Ag^{+} ion and Au^{3+} ions to the preformed AuNP and AgNP solutions, respectively. Clear aqueous MC flower extract is used as a reducing-cum-capping-cum-stabilising agent for the synthesis of metal nanoparticles. The structural, optical and plasmonic properties of synthesised nanoparticles have been studied through different instrumental techniques. The antibacterial activity of prepared nanoparticles is compared with aqueous extract using Gram positive *B. subtilis* and Gram negative *E. coli* bacteria, respectively.

Results and discussion

The aqueous extract of MC flowers is collected by digesting the clean flowers under microwave oven at 800 W followed by filtration (see Experimental section). The monometallic nanoparticles have been synthesised using metal precursors and plant extract in suitable ratios. The core–shell nanoparticles have been prepared by adding desired precursors to the preformed nanoparticles. The synthesis of metal nanoparticles using flower extract is outlined in Scheme 1. It is observed that the flower extract is sufficiently strong to reduce the metal ions into nanoparticles at room temperature.

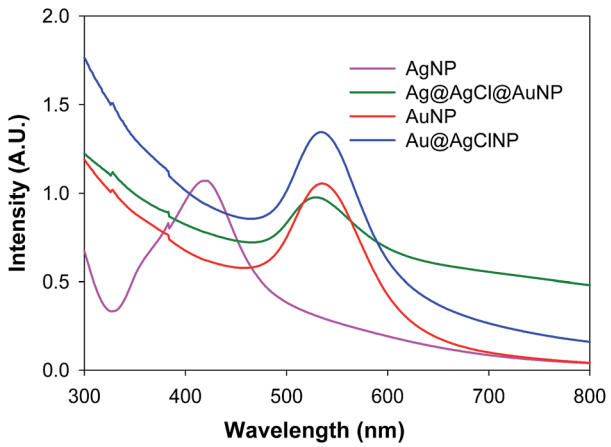

Fig. 1 UV-Vis spectra of the synthesised nanoparticles at room temperature. [Metal precursor] = 0.25 mM; plant extract = 50 μL in 10 mL.

The formation of monometallic AuNP (**NP1**) and AgNP (**NP2**), and their bimetallic core–shell type analogues Au@AgClNP (**NP3**) and Ag@AgCl@AuNP (**NP4**) utilising flower extract are monitored by observing their characteristic surface plasmon resonance (SPR) bands using UV-Vis spectroscopy (Fig. 1). The observed SPR bands at 435 nm and 530 nm in the UV-Vis spectra are the signature for the formation of AgNP and AuNP, respectively (Fig. 1). To optimise the reaction parameters, the concentration of the reagents, reaction time and pH are varied. It is found that at neutral pH, 50 μL plant extract with 0.25 mM concentration of $HAuCl_4$ in 10 mL exhibits a sharp SPR peak with the highest intensity at 530 nm (Fig. S1 and S2†). It is observed that within 10 minutes 90% of the reaction is completed and then the rate of reaction becomes very slow (Fig. S2b†). No significant change in the absorption maxima is observed even after 24 h. Interistingly, no significant change in the formation of AuNP is observed using the flower extract collected from different place and different time. This indicates the consistency of biological content of the flower extract and reproducibility and reliability over the batches (Fig. S3†). For AgNP, 6 h is found to be the optimum reaction time keeping other parameters same as AuNP (Fig. 1, S1b and S2c†). Hence, reaction times 3 h and 6 h are fixed for the preparation of AuNP and AgNP seeds, respectively, and are used for the preparation of their bimetallic analogues. To the *in situ* formed AgNP seed solution a varying amount aqueous $HAuCl_4$ solution is added. The strong SPR band of AgNP gets masked and concomitant growth of a new band at 530 nm is observed upon addition of Au^{3+} ions (Fig. 1 and S4b†). This suggests that AgNP surface is covered by Au atoms and may lead to the formation of core–shell type Ag@AuNP (**NP4**). Similarly, for Au@AgNP it is expected that the SPR band at 530 nm should get masked by Ag and a new SPR band should appear around 430 nm. However, the SPR band at 530 nm does not get masked rather the intensity gets increased continuously upon addition of Ag^{+} ions (Fig. 1 and S4a†) which is quite unusual. This suggests that deposition of Ag on AuNP seed does not proceed through expected way. Further, the literature reports suggest that Ag nanocube displays SPR band around 450–550 nm.[39–43] Thus, the formation of cubical Au@AgNP might be possible in the present case and the same is evident from the corresponding SEM images (*vide infra*). However, Ag nanocube should show additional SPR bands at 350 nm and 400 nm along with the peak at 530 nm which is absent in the present case.[44] Thus, the possibility of formation of Au@Ag nanocube might be ruled out. It is to be noted that after the formation of AuNP, the solution possesses a large amount of free Cl^{-} ions which can react with Ag^{+} and form AgCl. Hence, the other possibility of formation of cubical Au@AgClNP or Au@Ag/AgClNP should also be considered. As no SPR band around 400 nm is observed, the possibility of formation of Au@Ag/AgClNP can be eliminated. Hence, the composition of the bimetallic cubical nanoparticle may be assigned as Au@AgClNP (**NP3**). This observation is consistent

with earlier reports.[23] It is to be noted that there is no extra reducing agent or extract is required for the preparation of core–shell nanoparticles. The as-synthesised core–shell type Au@AgClNP is found to be stable at least upto one year in solution, however, Ag@AgCl@AuNP is degraded with time (Fig. S5†). Formation of cubical shape bimetallic nanoparticles *via* the simple addition of metal ion and plant extract is rare.[23] It is difficult to predict at the current stage which chemical constituent(s) is(are) responsible for the formation of nanocubes as plant extract consists of several phytochemicals. More studies are required to know the exact reason behind this observation.

The formation of nanoparticles, their morphology, shape and size have been authenticated by SEM analyses. From the SEM analyses, it is observed that the monometallic AuNP (**NP1**) and AgNP (**NP2**) are spherical in nature with average particle size 30 ± 5.0 nm and 50 ± 5.0 nm, respectively, using 50 μL extract and 0.25 mM metal ions (Fig. 2). Upon addition of second metal ion the size of the nanoparticles get enhanced and also changed the shape from spherical to cubical. It is to be noted that making large sized nanoparticle with variable shape and monodispersity using synthetic chemicals as reducing agent is very difficult. However, in the present case, using MC flower extract we are able to achieve cubical multimetallic nanoparticles by simple variation of concentration of metal ion indicating its significant role in making such shape. The presence of Au and Ag in monometallic and bimetallic nanoparticles have been evidenced through EDS analysis (Fig. 2).

The crystalline nature of the green synthesised nanoparticles are identified by powder X-ray diffraction (XRD) analyses coated on glass slides (Fig. 3). The XRD pattern of dried **NP1** and **NP2** have shown peaks at 38.20°, 44.50°, 64.70°, 77.70° and 82.10° which can be indexed as (111), (200), (220), (311) and (222) planes, suggesting the green synthesised nanoparticles are crystalline in nature.[43,45] Interestingly, the XRD pattern of core–shell nanoparticles (**NP3** and **NP4**) are found to be superimposable to individual **NP1** and **NP2** signals suggesting their crystalline nature too. In addition, additional peaks at 28.37°, 32.70°, 46.67°, 55.29°, 58.11°, 68.1° and 77.28° are also observed for bimetallic core–shell nanoparticles **NP3** and **NP4**. These peaks are consistent with the peaks observed for AgCl crystal, suggesting the presence of AgCl in the bimetallic core–shell

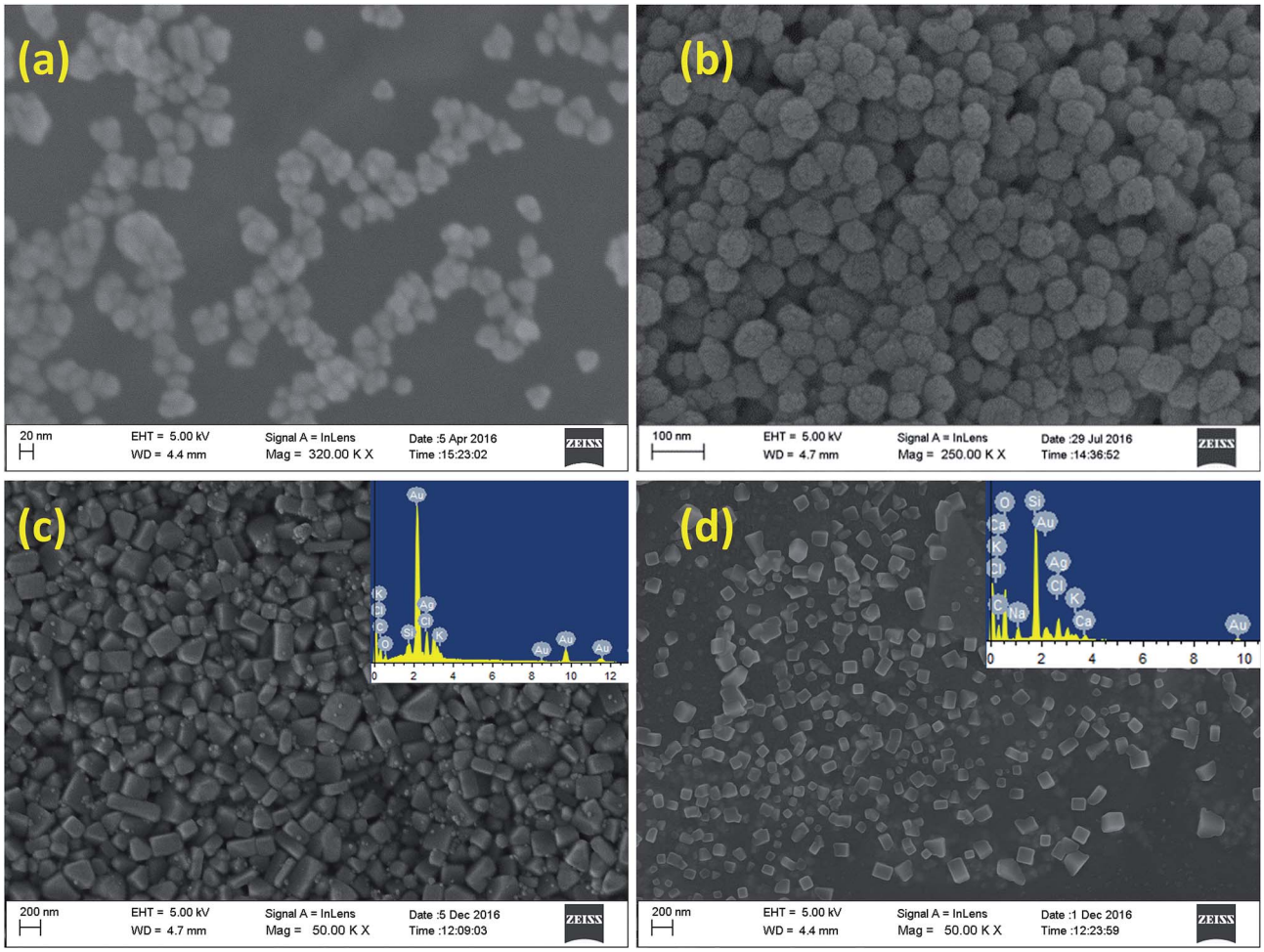

Fig. 2 FE-SEM images of (a) AuNPs, (b) AgNPs, (c) Au@AgClNPs and (d) Ag@AgCl@AuNPs prepared using MC flower extract at room temperature. Insets show EDS spectra of the corresponding nanoparticles.

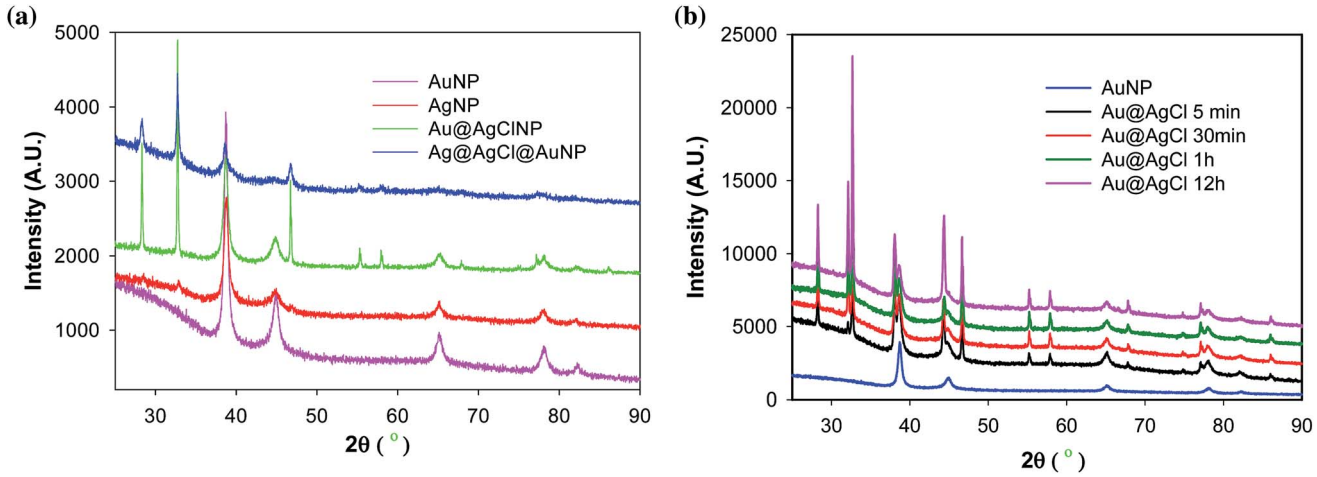

Fig. 3 Powder XRD spectra of (a) metal nanoparticles and (b) time-dependent spectra of Au@AgClNPs synthesised using MC flower extract.

nanoparticles. Thus, the composition of bimetallic core–shell nanoparticle **NP3** can be assigned as Au@AgClNP (Fig. 3).[38,46,47] The absence of SPR band of **NP3** at 400 nm related to AgNP in the UV-Vis spectrum (*vide supra*) also supports this assignment. A possible reason could be the availability of a large number of free Cl^- ions in solution after the formation AuNP, which lead to the formation of AgCl upon addition of $AgNO_3$. The crystallite size of the nanoparticles is calculated using the Debye–Scherrer equation (eqn (1)).

$$D = \frac{0.94\lambda}{\beta \cos \theta} \quad (1)$$

where D is the mean crystallite size, λ is the X-ray wavelength for CuK_α ($\lambda = 1.5406$ Å), β is full width at half maxima (FWHM) of diffraction peak of the plane (111) and θ is the diffraction angle. The average crystallite sizes are found to be 18–25 nm for **NP1**, 13–40 nm for **NP2**, 110–197 nm for **NP3** and 40–70 nm for **NP4** using eqn (1).

In the case of bimetallic nanoparticle **NP4**, the peak intensity corresponding to AgCl is very week (Fig. 3a). A possible reason could be the availability of small amount of Ag^+ ions which are formed during the oxidation of surface Ag^0. The Ag^+ ions then react with Cl^- of $HAuCl_4$ and form AgCl on top of AgNP. Hence, the composition of **NP4** may be assigned as Ag@AgCl@AuNP. As the formation of AgCl is prominent in the case of **NP3**, we further monitored the formation Au@AgClNP through powder X-ray diffraction studies with time. It is observed that the intensity of the peaks corresponding to AgCl are increased with time (Fig. 3b). This further confirms the assignment of Au@AgClNP for **NP3** and Ag@AgCl@AuNP for **NP4** although the amount of AgCl significantly varies in both cases.

To identify the probable biomolecules responsible for the reduction and stabilisation of nanoparticles present in the MC flower extract, FTIR analyses are performed (Fig. S6†). The dried MC flower extract has shown intense IR band at 3400 cm^{-1} and moderately intense bands at 1618 cm^{-1}, 1352 cm^{-1}, 1218 cm^{-1} and 1046 cm^{-1} indicating the presence of (N–H or O–H), C–H, C═O, C═C, C–O, C–OH, C–N functional groups, respectively. The band at 1218 cm^{-1} gets vanished and shift of the other bands are also observed after the formation of nanoparticles. It is difficult to exactly identify the biomolecule(s) responsible for the reduction of metal ion. However, the previous reports and the present FTIR results suggest the N–H or O–H group present in the plant extract are responsible for stabilising and reducing the nanoparticles.[36–38]

AgNP is known to exhibit good antibacterial activity. However, the exploration of antibacterial activity of bimetallic nanoparticles is limited.[48,49] To test the antibacterial potency of our synthesised nanoparticles, disc diffusion assay of Gram negative *E. coli* and Gram positive *B. subtilis* strains are used. The preliminary screening study by disc diffusion assay demonstrates that AuNP (**NP1**) does not possess any antibacterial activity whereas monometallic AgNP (**NP2**), bimetallic Au@AgClNP (**NP3**) and Ag@AgCl@AuNP (**NP4**) are found to be active (Fig. 4). The disk diffusion assay have shown a zone of inhibition of 2.8 mm, 4.5 mm and 3.4 mm for *E. coli* and 4.3 mm, 4.6 mm, and 0.0 mm for *B. subtilis*, respectively, for **NP2**, **NP3** and **NP4** (Fig. 4a and Table 1). Among the nanoparticles, the core–shell type **NP3** has shown the best activity against both *E. coli* and *B. subtilis*, although the standard drug kanamycin is inactive (against *B. subtilis*) (Fig. 4 and S6†). It should be noted that MC flower extract and chemically synthesised AuNP and AgNP (using $NaBH_4$ and PEG) do not show any antibacterial activity (Fig. 4a). Next, we have studied the growth kinetics of *E. coli* and *B. subtilis* strains using active nanoparticles. The growth of the strains has been monitored by measuring the OD at 600 nm (OD_{600}) in 1 h interval. Results indicate that **NP3** completely inhibit the growth of *E. coli* and *B. subtilis*, which is similar to the standard antibiotics kanamycin on *E. coli* and ampicillin on *B. subtilis* (Fig. 4b). The bimetallic **NP4** has also shown moderate growth inhibition of *E. coli*. The monometallic **NP2** does not show any effect on the growth kinetics of *E. coli*, however, has a little effect on *B. subtilis* (Fig. 4b).

The minimum inhibitory concentration (MIC) and minimum bactericidal concentration (MBC) of the active nanoparticles have been determined. The MIC and MBC values are found to be 25 μM

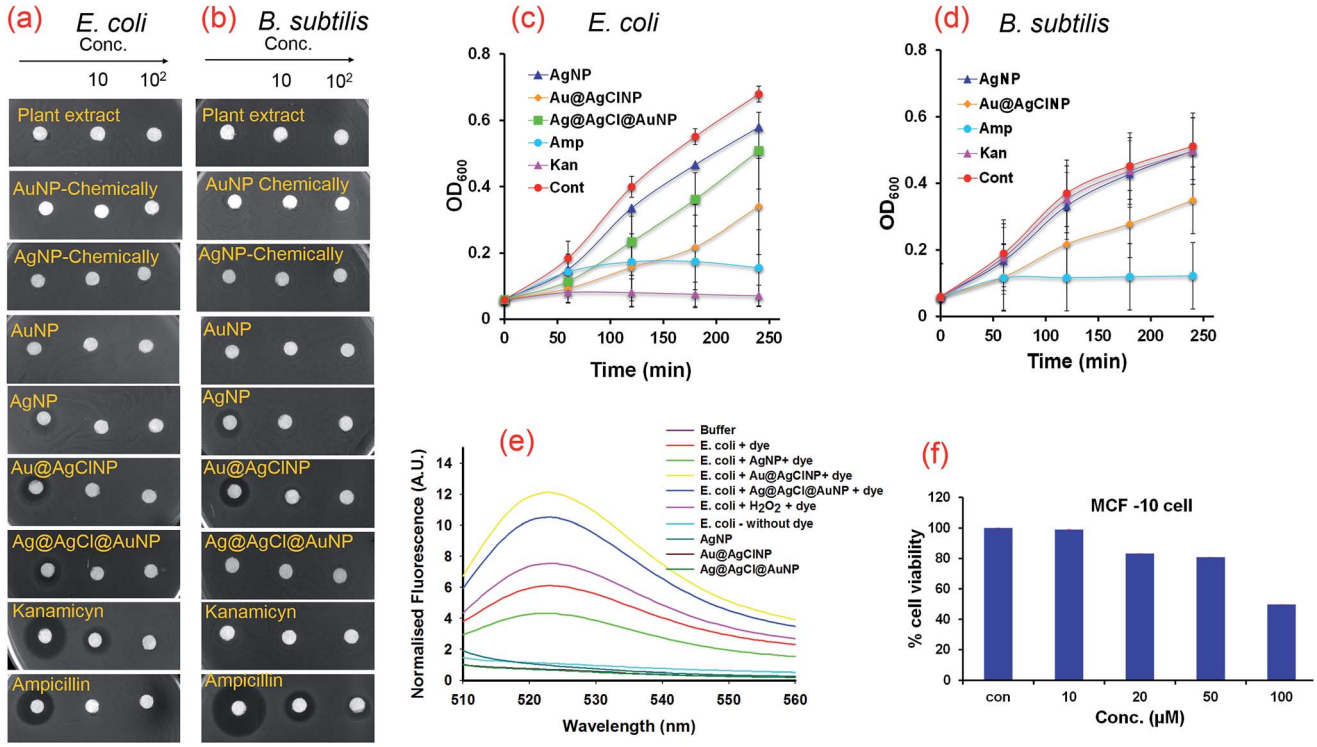

Fig. 4 Screening of antibacterial activity against *E. coli* and *B. subtilis* of green synthesised nanoparticles by (a and b) disc diffusion assay and (c and d) growth curve assay. (e) Nanoparticle induced intracellular ROS production on *E. coli* and (f) *in vitro* cytotoxicity assay of Au@AgClNP against normal human breast (MCF-10) cell line.

Table 1 *In vitro* growth inhibition (MIC) and bacteriostatic (MBC) concentration of the green synthesised nanoparticles against *E. coli* and *B. subtilis* strains. Concentration are in μM and zone inhibition areas are in mm

	E. coli			*B. subtilis*		
NPs	Zone inhibition	MIC	MBC	Zone inhibition	MIC	MBC
AgNP (**NP2**)	2.8	50	ND	4.3	28	ND
Au@AgClNP (**NP3**)	4.5	25	31	4.6	15	25
Ag@AgCl@AuNP (**NP4**)	3.4	28	37	—	—	—
Kanamycin	8.6	8.7	5	—	ND	ND
Ampicillin	7.2	14	10	12.9	2.5	2.5

and 31 μM for **NP3**, 28 μM and 37 μM for **NP4** against *E. coli*, and 15 μM and 25 μM for **NP3** against *B. subtilis*, respectively (Table 1 and Fig. S7†). The growth curve and MIC/MBC values suggest that **NP3** and **NP4** for *E. coli* and **NP3** for *B. subtilis* are acting as bactericidal. **NP2** does not have any significant effect on growth curve, however, it is significant in disc diffusion assay, possibly due to prolong incubation time (16 h).

Next we have studied the mechanism of antibacterial activity of nanoparticles towards *E. coli*. It is known that reactive oxygen species (ROS) plays a crucial role in bacterial cell death. Metal nanoparticles are known to induce ROS production and alter the cell metabolism at different levels like transcription, transport and membrane integrity in bacteria.[27,50] The production of ROS through primary antibacterial mechanism after the treatment of nanoparticles is measured using DCFDA fluorescent dye. *E. coli* stains are treated with nanoparticles at MIC concentrations for 1 h followed by addition of DCFDA dye for 30 min. DCFDA de-esterified by cellular enzymes and oxidized to DCF in presence of ROS, which has higher fluorescence intensity. The ROS is determined by measuring the fluorescence intensity as described in the Experimental section.

It is observed that bimetallic core–shell Au@AgClNP (**NP3**) and Ag@AgCl@AuNP (**NP4**) induce more ROS production than monometallic AgNP (**NP2**) and positive control on *E. coli* (Fig. 4e). The order of ROS production is **NP3** > **NP4** > **NP2**. The observed antibacterial activity of the nanoparticles are also in the order ROS production. Thus, nanoparticles induced ROS formation is primarily responsible for bacterial cell death.

Prompted by this exciting antibacterial activity of **NP3** we become interested to study its toxic effect towards normal

human cells. Normal human breast cell (MCF-10) has been selected for toxicity study. It is observed that there is no inhibition effect of **NP3** towards the growth of MCF-10 cells (IC_{50} > 100 μM) (Fig. 4f). This indicates that the nanoparticle has no/less toxic effect on human cell.

Conclusions

In conclusion, the present study demonstrates successful synthesis of monometallic AuNP and AgNP, and bimetallic Au@AgClNP and Ag@AgCl@AuNP core–shell nanoparticles using flower extract of *Muntingia calabura*. The synthesised nanoparticles have been characterised using various analytical techniques. The formation of nanoparticles have been confirmed by observing the characteristic SPR bands using UV-Vis spectroscopy. The electron microscopic images and EDS analysis suggests the spherical shape monometallic and cubical shape bimetallic nanoparticles and presence of desired elements, respectively. The antibacterial study against *E. coli* and *B. subtilis* shows that AuNP is inactive whereas AgNP, core–shell type Au@AgClNP and Ag@AgCl@AuNP are effective. The Au@AgClNP has shown the best antibacterial activity among the present set of nanoparticles and the activity is comparable to the commercially available kanamycin or ampicillin. Our results show that increased antibacterial activity of bimetallic compounds Au@AgClNP or Ag@AgCl@AuNP is due to increased production of ROS which is the primary component to alter the metabolic state of *E. coli*. Moreover, the core–shell type Au@AgClNP shows significantly less toxicity (IC_{50} > 100 μM against MCF-10 normal cell line). Achieving anisotropic nanoparticles is cumbersome. The present study demonstrates such an example of the preparation of cubic nanoclusters by simple and milder process. Moreover, the synthesised multimetallic nanoparticles show significantly good antibacterial activity and less cytotoxicity towards normal human cell which is a remarkable observation. Thus, we believe that the present set of examples is an important addition to the community those who are working on the development of anisotropic nanostructures and antibacterial agents for tropical applications.

Experimental

Materials

The chemicals $HAuCl_4$ and $AgNO_3$ were purchased from Sigma-Aldrich, India. All the experiments were performed in triple distilled water. All the glasswares were cleaned with aqua regia to remove the traces of metal contaminant and thoroughly washed with triple distilled water followed by drying in the oven.

Preparation of *Muntingia calabura* flower extract

10 g fresh flower of *Muntingia calabura* were collected from the parking lot of Siksha 'O' Anusandhan University, washed with ethanol for 30 s followed by thorough wash with triple distilled water. The clean flowers were soaked in 50 mL triple distilled water and boiled in a microwave oven at 800 W for 1 minute. This process was repeated for 6 times in 1 h interval. This was then allowed to cool to room temperature and filtered. The filtrate was then centrifuged at 14 000 rpm for 40 minutes at 4 °C. The supernatant was collected and stored at −20 °C and used as stock solution. The extract was allowed to pass through 0.2 μm syringe filter before its use for the reduction of metal ions.

Synthesis of monometallic AuNP (NP1) and AgNP (NP2)

A 100 μL, 25 mM aqueous solution of $HAuCl_4$ was added to triple distilled water and stirred for 30 minutes at room temperature. To the mixture, a varying amount of aqueous flower extract of *Muntingia calabura* (25 μL, 50 μL and 100 μL) were added with stirring. The final volume of the reaction mixture was maintained 10 mL by pre-adjusting the volume of water. The colour of the solution was gradually changed from light yellow to violet to purple indicating the formation of AuNP. The progress of the reaction was monitored by UV-Vis spectrometer by measuring the characteristic SPR band of AuNP at 530 nm with time. Similar synthesis procedure was followed for the preparation of AgNP. The synthesised nanoparticles solution were kept in the refrigerator and used as stock solution.

Synthesis of bimetallic Au@AgClNP (NP3) and Ag@AgCl@AuNP (NP4)

The aforementioned AuNP and AgNP solution were taken as seeds for the preparation of bimetallic core–shell type nanoparticles.

To 10 mL AuNP seed solution variable concentrations (0.05 mM, 0.1 mM, 0.2 mM, 0.4 mM, 0.6 mM, 0.7 mM and 1.0 mM) of aqueous $AgNO_3$ solution were added separately with stirring and continued for 6 h at room temperature. The formation of core–shell Au@AgClNP was monitored by UV-Vis spectroscopy. The nanoparticle solution was kept in the refrigerator for further use.

Similarly, Ag@AgCl@AuNP was synthesised by separately adding variable concentrations (0.0062 mM, 0.0125 mM, 0.025 mM, 0.05 mM, 0.1 mM, 0.2 mM and 0.4 mM) of aqueous $HAuCl_4$ solution to 10 mL AgNP seed solution. The solution was stirred for 6 h at room temperature and kept in refrigerator for further use.

Chemical synthesis of AuNP and AgNP

Metal nanoparticles were synthesised chemically by using sodium borohydride as reducing agent and PEG-6000 as stabilising agent to compare the activity with green synthesised nanoparticles. In brief, 100 μL, 0.5 mg mL^{-1} $NaBH_4$ solution was added dropwise to an ice cold vigorously stirred 10 mL 0.25 mM $HAuCl_4$ solution containing 200 μL PEG-6000 (0.1% w/v final concentration). The colour of the solution immediately got changed and stirring was continued for another 2 h and stored in the refrigerator for further use. Similar procedure was followed for the synthesis of AgNP.

Characterisation

UV-Vis spectroscopic studies. Initial characterisation of different metal nanoparticles were investigated by UV-Vis spectroscopy using Perkin Elmer Lambda 35 spectrophotometer. The spectral data obtained were then plotted using Sigma Plot 10.0.

Powder X-ray diffraction (XRD) analysis. Monometallic **NP1** and **NP2**, and bimetallic **NP3** and **NP4** were concentrated by centrifugation. The concentrated nanoparticles were then placed on glass slides followed by dried at 70 °C overnight. The X-ray diffraction analyses were performed using Bruker D8 Advance Diffractometer (Bruker AXS, Germany) with Cu K_α radiation (λ = 1.54 Å). XRD patterns of nanoparticles were recorded over a 2θ range of 10–90° with a scan rate of 0.0438 deg S^{-1}. The instrument was calibrated with lanthanum hexaboride (LaB_6) prior to analysis.

Fourier transform infrared spectroscopy (FTIR) studies. To find out the presence of biomolecules responsible for the reduction and capping of metal nanoparticles, FTIR (Bruker FTIR ALPHA) analyses were performed using dried *Muntingia calabura* flower extract and metal nanoparticles (AuNP and AgNP) by making KBr pellets.

Scanning electron microscopy (SEM) studies. For SEM analysis, samples were placed on carbon tape and dried. The SEM images were recorded using Scanning Electron Microscope (Zeiss Merlin compact Microscope, Oxford instruments).

Antibacterial activity study

E. coli MG1655 and *B. subtilis* 168 strains were used for all antimicrobial assays. Luria–Bertani broth (Himedia, India) was used for disc diffusion assay and growth curve measurements. Mueller–Hinton broth/Agar (Himedia, India) was used for MIC and MBC determinations. Whatman filter paper disks (diameter = 5 mm) (Sigma-Aldrich, USA) were prepared and autoclaved before use. Ampicillin and kanamycin antibiotics were procured from Sigma-Aldrich, USA. All nanoparticles, antibiotics were diluted in double distilled water. B. D falcon non-treated 24 and 96 well culture plates (BD Bioscience, India) were used in experiments.

Disk diffusion assay

Overnight culture of *E. coli* and *B. subtilis* strains were diluted to OD_{600} 0.05. From that, 2 mL of culture was poured on each LB agar plate and immediately excess culture was discarded. Plates were air-dried. Filter paper disks were placed on dried culture LB agar plate. 40 μL of AgNP, AuNP, Au@AgClNP and Ag@AgCl@AuNP (0.25 mM) was spotted on paper disks and air-dried for 30 min. The same concentration of ampicillin and kanamycin (0.25 mM) and MC flower extract (40 μL) were taken as controls. Chemically synthesised AgNP and AuNP were also taken as controls. After that, plates were incubated at 37 °C for 10 h. Clear zones were noted as the inhibitory effect of nanoparticles on growing lane of culture.

Growth curve assay

E. coli, *B. subtilis* cultures were diluted to OD_{600} 0.1 and final concentration of 50 μM nanoparticles were added to 500 μL of culture in 24 well multi-well plates. For controls, equal concentrations of ampicillin and kanamycin were added. Plates were incubated at 37 °C with shaking at 200 rpm. OD_{600} of culture was measured at each hour with Varioskan multi-well plate reader.

MIC and MBC determination

MIC was determined using microdilution method according to the guidelines of CLSI protocol.[51] *E. coli* and *B. subtilis* strains were grown up to 0.5 OD_{600} at 37 °C. The culture was diluted to OD_{600} 0.0005 ($\sim 5 \times 10^5$ cells per mL) and 100 μL were added to the different wells in 96 well plate. Different concentrations of nanoparticles (6 μM to 137 μM) were prepared in distilled water and added to the each well. Ampicillin and kanamycin were also tested as controls. The plate was incubated at 37 °C for 16 h with shaking at 200 rpm. MIC noted as the concentration at which no visible growth observed. MBC was determined by spotting the culture from MIC plate on fresh MH agar plate and incubated at 37 °C for 12 h. MBC was noted as the concentration at which no growth was observed on the plate.

ROS measurement

E. coli culture was grown at 37 °C until OD_{600} reaches ~0.2 and nanoparticles (Ag or Au@AgCl or Ag@AgCl@Au) were added separately to culture at MIC concentrations. Further, the culture was grown for 1 h at 37 °C, 20 μM of DCFDA (2′,7′-dichlorofluorescin diacetate) (Sigma-Aldrich, USA) was added and incubated at 37 °C for 30 minutes. The culture was diluted to 15 times in 20 mM of phosphate buffer saline (PBS). The emission spectra were recorded from 510–560 nm using PTI-fluorometer with an excitation at 495 nm at 25 °C. For positive control, *E. coli* treated with H_2O_2 was taken along with DCFDA dye.

Cellular toxicity assay

Normal human breast cells (MCF-10A) (from the ATCC) were cultured in serum-free mammary epithelial growth medium (MEGM; Clonetics Corp.) supplemented with 100 ng mL^{-1} cholera toxin. Normal human mammary epithelial cells (from Clonetics Corp.) were maintained in MEGM supplemented with bovine pituitary extract, insulin, human epidermal growth factor, hydrocortisone, and antibiotics. The cell viability of the green synthesised Au@AgClNP was assayed by standard MTT (3-(4,5-dimethylthiazol-2-yl)-2-5-diphenyl tetrazolium bromide) assay by following the procedure reported earlier.[52]

Acknowledgements

N. P. would like to acknowledge Siksha 'O' Anusandhan University for her doctoral fellowship. S. P. would like to acknowledge Council of Scientific and Industrial Research (Letter No. 01(2692)/12/EMR-II dated 03/10/2012) New Delhi for financial support. TKB thanks DBT for Ramalingaswami fellowship and financial assistance from Department of Biotechnology, India (BT/PR5430/MED/29/566/2012). We thank the reviewers for their constructive suggestions and critical comments during revision stage to improve the quality of the manuscript.

Notes and references

1 J. Luo, M. M. Maye, Y. Lou, L. Han, M. Hepel and C. J. Zhong, *Catal. Today*, 2002, **77**, 127–138.
2 W. L. Barnes, A. Dereux and T. W. Ebbesen, *Nature*, 2003, **424**, 824–830.
3 M. C. Daniel and D. Astruc, *Chem. Rev.*, 2004, **104**, 293–346.
4 Y. Yang, S. Matsubara, L. Xiong, T. Hayakawa and M. Nogami, *J. Phys. Chem. C*, 2007, **111**, 9095–9104.
5 M. De, P. S. Ghosh and V. M. Rotello, *Adv. Mater.*, 2008, **20**, 4225–4241.
6 D. A. Giljohann, D. S. Seferos, W. L. Daniel, M. D. Massich, P. C. Patel and C. A. Mirkin, *Angew. Chem., Int. Ed.*, 2010, **49**, 3280–3294.
7 S. Fazal, A. Jayasree, S. Sasidharan, M. Koyakutty, S. V Nair and D. Menon, *ACS Appl. Mater. Interfaces*, 2014, **6**, 8080–8089.
8 A. K. Khan, R. Rashid, G. Murtaza and A. Zahra, *Trop. J. Pharm. Res.*, 2014, **13**, 1169–1177.
9 R. Jin, Y. C. Cao, E. Hao, G. S. Métraux, G. C. Schatz and C. A. Mirkin, *Nature*, 2003, **425**, 487–490.
10 M. Rycenga, C. M. Cobley, J. Zeng, W. Li, C. H. Moran, Q. Zhang, D. Qin and Y. Xia, *Chem. Rev.*, 2011, **111**, 3669–3712.
11 M. Sardar, A. Mishra and R. Ahmad, *Biosens. Nanotechnology*, Scrivener Publ., USA, 2014, pp. 239–266.
12 J. Xie, J. Y. Lee, D. I. C. Wang and Y. P. Ting, *Small*, 2007, **3**, 672–682.
13 J. Xie, J. Y. Lee, D. I. C. Wang and Y. P. Ting, *ACS Nano*, 2007, **1**, 429–439.
14 Y. Zhou, W. Lin, J. Huang, W. Wang, Y. Gao, L. Lin, Q. Li, L. Lin and M. Du, *Nanoscale Res. Lett.*, 2010, **5**, 1351.
15 L. P. Silva, I. G. Reis and C. C. Bonatto, in *Green Processes for Nanotechnology*, Springer, 2015, pp. 259–275.
16 S. S. Shankar, A. Rai, B. Ankamwar, A. Singh, A. Ahmad and M. Sastry, *Nat. Mater.*, 2004, **3**, 482–488.
17 S. P. Chandran, M. Chaudhary, R. Pasricha, A. Ahmad and M. Sastry, *Biotechnol. Prog.*, 2006, **22**, 577–583.
18 A. Tripathy, A. M. Raichur, N. Chandrasekaran, T. C. Prathna and A. Mukherjee, *J. Nanopart. Res.*, 2010, **12**, 237–246.
19 D. Philip, *Spectrochim. Acta, Part A*, 2011, **78**, 327–331.
20 S. Phukan, P. Bharali, A. K. Das and M. H. Rashid, *RSC Adv.*, 2016, **6**, 49307–49316.
21 S. K. Nethi, S. Mukherjee, V. Veeriah, A. K. Barui, S. Chatterjee and C. R. Patra, *Chem. Commun.*, 2014, **50**, 14367–14370.
22 S. Mukherjee, M. Dasari, S. Priyamvada, R. Kotcherlakota, V. S. Bollu and C. R. Patra, *J. Mater. Chem. B*, 2015, **3**, 3820–3830.
23 S. Balasubramanian, S. R. Bezawada and R. Dhamodharan, *ACS Sustainable Chem. Eng.*, 2016, **4**, 2960–2968.
24 A. Sahoo, S. K. Tripathy, N. Dehury and S. Patra, *J. Mater. Chem. A*, 2015, **3**, 19376–19383.
25 Y. Kang, J. Snyder, M. Chi, D. Li, K. L. More, N. M. Markovic and V. R. Stamenkovic, *Nano Lett.*, 2014, **14**, 6361–6367.
26 S. Patra and H. Yang, *Bull. Korean Chem. Soc.*, 2009, **30**, 1485–1488.
27 K. Zheng, M. I. Setyawati, T. P. Lim, D. T. Leong and J. Xie, *ACS Nano*, 2016, **10**, 7934–7942.
28 M. P. Correa, *Diccionário das plantas úteis do Brasil e das exóticas cultivadas*, 1931.
29 J. F. Morton, *Fruits warm Clim.*, 1987, vol. 2, pp. 65–69.
30 Y. C. Wee, Singapore Singapore Sci. Cent, 160p.-col. illus., ISBN.
31 B.-N. Su, E. J. Park, J. S. Vigo, J. G. Graham, F. Cabieses, H. H. S. Fong, J. M. Pezzuto and A. D. Kinghorn, *Phytochemistry*, 2003, **63**, 335–341.
32 Z. A. Zakaria, S. Mustapha, M. R. Sulaiman, A. M. Mat Jais, M. N. Somchit and F. C. Abdullah, *Med. Princ. Pract.*, 2007, **16**, 130–136.
33 N. Kaneda, J. M. Pezzuto, D. D. Soejarto, A. D. Kinghorn, N. R. Farnsworth, P. Tuchinda, J. Udchachon, T. Santisuk and V. Reutrakul, *Planta Med.*, 1990, **56**, 672–673.
34 C. M. Nshimo, J. M. Pezzuto, A. D. Kinghorn and N. R. Farnsworth, *Int. J. Pharmacogn.*, 1993, **31**, 77–81.
35 Z. A. Zakaria, A. S. Sufian, K. Ramasamy, N. Ahmat, M. R. Sulaiman, A. K. Arifah, A. Zuraini and M. N. Somchit, *Afr. J. Microbiol. Res.*, 2010, **4**, 304–308.
36 M. Ahmaruzzaman and S. B. T. Babita Devi, *New J. Chem.*, 2016, **40**, 1497–1506.
37 J. Grover and S. Yadav, *J. Ethnopharmacol.*, 2004, **93**, 123–132.
38 T. B. Devi, S. Begum and M. Ahmaruzzaman, *J. Photochem. Photobiol., B*, 2016, **160**, 260–270.
39 A. R. Siekkinen, J. M. McLellan, J. Chen and Y. Xia, *Chem. Phys. Lett.*, 2006, **432**, 491–496.
40 A. Moreau, C. Ciracì, J. J. Mock, R. T. Hill, Q. Wang, B. J. Wiley, A. Chilkoti and D. R. Smith, *Nature*, 2012, **492**, 86–89.
41 A. A. AbdelHamid, M. A. Al-Ghobashy, M. Fawzy, M. B. Mohamed and M. M. S. A. Abdel-Mottaleb, *ACS Sustainable Chem. Eng.*, 2013, **1**, 1520–1529.
42 Q. Zhang, W. Li, C. Moran, J. Zeng, J. Chen, L.-P. Wen and Y. Xia, *J. Am. Chem. Soc.*, 2010, **132**, 11372–11378.
43 N. M. Kha, C. H. Chen, W. N. Su and J. Rick, *Phys. Chem.*, 2015, **17**, 21226.
44 B. Wiley, Y. Sun, B. Mayers and Y. Xia, *Chem.–Eur. J.*, 2005, **11**, 454–463.
45 P. Kannan and S. A. John, *Nanotechnology*, 2008, **19**, 85602.
46 J. Song, J. Roh, I. Lee and J. Jang, *Dalton Trans.*, 2013, **42**, 13897–13904.
47 C. Han, L. Ge, C. Chen, Y. Li, Z. Zhao, X. Xiao, Z. Li and J. Zhang, *J. Mater. Chem. A*, 2014, **2**, 12594–12600.
48 D. Huo, J. He, H. Li, H. Yu, T. Shi, Y. Feng, Z. Zhou and Y. Hu, *Colloids Surf., B*, 2014, **117**, 29–35.
49 S. Yallappa, J. Manjanna and B. L. Dhananjaya, *Spectrochim. Acta, Part A*, 2015, **137**, 236–243.
50 K. Zheng, M. I. Setyawati, D. T. Leong and J. Xie, *ACS Nano*, 2017, DOI: 10.1021/acsnano.7b02035.
51 F. R. Cockerill III, M. A. Wikler, J. Alder, M. N. Dudley, G. M. Eliopoulos, M. J. Ferraro, D. K. Hardy, D. W. Hecht, J. A. Hindler and J. B. Patel, *Methods Dilution Antimicrob. Susceptibility Tests Bact. That Grow Aerob. Approv. Stand.*, Clin. Lab. Stand. Institute, Wayne, 9th edn, 2009, vol. 31, CLSI Doc.
52 S. K. Tripathy, U. De, N. Dehury, S. Pal, H. S. Kim and S. Patra, *Dalton Trans.*, 2014, **43**, 14546–14549.

